Processes of 30–90 days sea surface temperature variability in the northern Indian Ocean during boreal summer

J. Vialard · A. Jayakumar · C. Gnanaseelan · M. Lengaigne · D. Sengupta · B. N. Goswami

Abstract During summer, the northern Indian Ocean exhibits significant atmospheric intraseasonal variability associated with active and break phases of the monsoon in the 30–90 days band. In this paper, we investigate mechanisms of the Sea Surface Temperature (SST) signature of this atmospheric variability, using a combination of observational datasets and Ocean General Circulation Model sensitivity experiments. In addition to the previously-reported intraseasonal SST signature in the Bay of Bengal, observations show clear SST signals in the Arabian Sea related to the active/break cycle of the monsoon. As the atmospheric intraseasonal oscillation moves northward, SST variations appear first at the southern tip of India (day 0), then in the Somali upwelling region (day 10), northern Bay of Bengal (day 19) and finally in the Oman upwelling region (day 23). The Bay of Bengal and Oman signals are most clearly associated with the monsoon active/break index, whereas the relationship with signals near Somali upwelling and the southern tip of India is weaker. In agreement with previous studies, we find that heat flux variations drive most of the intraseasonal SST variability in the Bay of Bengal, both in our model (regression coefficient, 0.9, against ∼0.25 for wind stress) and in observations (0.8 regression coefficient); ∼60% of the heat flux variation is due do shortwave radiation and ∼40% due to latent heat flux. On the other hand, both observations and model results indicate a prominent role of dynamical oceanic processes in the Arabian Sea. Wind-stress variations force about 70–100% of SST intraseasonal variations in the Arabian Sea, through modulation of oceanic processes (entrainment, mixing, Ekman pumping, lateral advection). Our ∼100 km resolution model suggests that internal oceanic variability (i.e. eddies) contributes substantially to intraseasonal variability at small-scale in the Somali upwelling region, but does not contribute to large-scale intraseasonal SST variability due to its small spatial scale and random phase relation to the active-break monsoon cycle. The effect of oceanic eddies; however, remains to be explored at a higher spatial resolution.

J. Vialard (✉) · M. Lengaigne
Laboratoire d'Océanographie Expérimentation et Approches Numériques (LOCEAN), Case 100, CNRS, IRD, Univerité P. et M. Curie, 4, Place Jussieu, 75252 Paris Cedex 05, France
e-mail: jerome.vialard@locean-ipsl.upmc.fr

A. Jayakumar · C. Gnanaseelan · B. N. Goswami
Indian Institute of Tropical Meteorology, Pune, India

M. Lengaigne
National Institute of Oceanography, CSIR, Goa, India

D. Sengupta
Centre of Atmospheric and Oceanic Sciences, Indian Institute of Sciences, Bangalore, India

1 Introduction

The livelihood of over one billion people in the Indian subcontinent is affected by the amount of rain falling during the Southwest monsoon. The quantity of food produced in India is indeed highly correlated with monsoon rainfall (e.g. Webster et al. 1998). The monsoon itself does not come as a single, long downpour, but is modulated at intraseasonal timescales by "active" (or rainy) and "break" (or dry) periods (see Goswami 2005 for a review).

It is important to understand these active and break phases of the monsoon from two perspectives. First, it has been demonstrated that intraseasonal variability of rainfall is perhaps as important as the total seasonal rainfall for agriculture (e.g. seeds planted before a break phase are generally lost, Gadgil 2003; Ingram et al. 2002). Secondly, the amount of internally driven interannual variability of the monsoon seems to be largely due to intraseasonal variability of the monsoon (Ajaya Mohan and Goswami 2003).

There are two clear peaks of atmospheric variability at 10–20 and 30–90 days variability over the northern Indian Ocean in summer (Goswami 2005). The 10–20 days variability originates from the western Pacific and propagates westward to the Indian Ocean. It has a low-level wind structure characteristic of a first meridional mode baroclinic Rossby wave, with a 5° northward shift of the line of symmetry due to mean summer atmospheric flow (Chatterjee and Goswami 2004). The amplitude of the SST response to the 30–90 days variability is largest (e.g. Sengupta et al. 2001, Duvel and Vialard 2007), and we hence focus on this timescale in the present paper. The 30–90 days variability is associated with active and break phases of the Indian Monsoon. During active phases, there is a strengthening of the monsoon jet, increased rainfall over India and increased deep atmospheric convection over the eastern Arabian Sea and the Bay of Bengal (e.g. Goswami and Ajaya Mohan 2001; Annamalai and Slingo 2001; Webster et al. 1998; Joseph and Sijikumar 2004). During the break phase, increased convection and rainfall are located over the ocean south of India, and the low-level jet is deflected to the south, resulting in decreased wind over the Arabian Sea, India and the Bay of Bengal. The maximum convective perturbation propagates northward, going from about 5°N (break phase) to the northern Bay of Bengal (about 20°N) in 20 days (Goswami 2005). In terms of mechanisms, the 30–90 day mode is essentially atmospheric, resulting from the interaction of atmospheric dynamics and convection. The northward propagation of the precipitation is caused by atmospheric boundary-layer convergence north of the maximum of convection (Lawrence and Webster 2002; Goswami 2005).

While summer intraseasonal variability over the northern Indian Ocean largely arises from coupling between large-scale atmospheric dynamics and deep convection, it has a very clear surface signature. There are clear near surface wind variations that induce changes in both upper ocean mixing and latent heat fluxes uptake. At the same time, changes in deep atmospheric convection modulate downward solar irradiance. Sengupta and Ravichandran (2001) showed relatively large amplitude (1–1.5°C) SST changes with 30–40-day period in the northern Bay of Bengal during the Southwest Monsoon as a result. These

SST variations are however, poorly captured by infrared SST estimates because of masking by clouds associated with deep atmospheric convection. Because of this, early papers trying to address that variability generally suggested relatively weak amplitude of intraseasonal SST variability in the northern Indian Ocean (e.g. Krishnamurti et al. 1988; Hendon and Glick 1997; Shinoda and Hendon 1998).

The more recent availability of microwave SST measurements, which are less sensitive to masking by clouds than infrared measurements (Wentz et al. 2000), provides a better representation of SST signals associated with the monsoon active-break cycles. Sengupta et al. (2001), Vecchi and Harisson (2002) and Duvel and Vialard (2007) showed that the 1–2°C peak-to-peak SST variations extend throughout the northern Bay of Bengal and south China sea, and propagate northward along with the deep atmospheric convection and surface flux perturbations. Sengupta and Ravichandran (2001) and Duvel and Vialard (2007) attributed most of these SST changes to forcing by atmospheric heat fluxes.

Modelling studies also investigated the SST signature of the active and break phases over the Bay of Bengal. Fu et al. (2003) used a hybrid coupled general circulation model, in which the SST response in the Bay of Bengal is dominated by surface heat flux forcing (about two third of the response), with entrainment into the mixed layer being non-negligible (see their Fig. 6). Waliser et al. (2004) used an Ocean General Circulation Model (OGCM) forced with a canonical MJO perturbation and showed (their Fig. 14) that net heat fluxes drive the SST intraseasonal variations in the Bay of Bengal with occasional significant contributions from the subsurface ocean (vertical advection and entrainment). In Bellon et al. (2008) simple coupled model, net heat flux is the primary contributor to intraseasonal SST perturbations, with a non-negligible contribution from vertical advection (their Fig. 7). Duncan and Han (2009) suggest that in the Bay of Bengal, latent heat flux variations have a stronger influence on SST than upwelling and advection induced by wind stress. Most studies hence suggest that SST changes in the Bay of Bengal are dominated by heat fluxes, with exchanges with the subsurface contributing to a varying extent.

In comparison with the numerous studies focussing on the Bay of Bengal intraseasonal SST variations associated with monsoon and active break phases, there are only a few studies in the Arabian Sea. Analyses of the large-scale SST response to intraseasonal atmospheric variability in Duvel and Vialard (2007) show signals over the western Arabian sea but do not analyse them in detail. Roxy and Tanimoto (2007) identify SST variations along the west coast of India and in the Somali and Oman upwelling regions, and hypothesize that these SST perturbations contribute to the Northward propagation of the active-break cycle by

helping to destabilize the northern flank of the convectively active region. The composites in Joseph and Sabin (2008) also clearly show signals in the Arabian Sea, but the authors focus on the potential feedbacks of SST variations in the Bay of Bengal on the active-break monsoon cycle.

This study has two objectives. First, provide a more detailed description of SST variations associated with active and break monsoon phases over the Arabian Sea. Second, quantify the respective contributions of atmospheric heat fluxes and oceanic processes in the intraseasonal (30–90 days) SST response over both the Arabian Sea and Bay of Bengal. In a companion paper, we used a combination of observations and OGCM experiments to understand processes of intraseasonal variability in the 5°S–10°S band of the Indian Ocean during boreal winter (Jayakumar et al. 2011). In this paper, we will use a similar strategy to investigate these processes over the northern Indian Ocean during boreal summer. Section 2 presents the data, methodology and description of modelling experiments. In Sect. 3, we validate the model mean state during boreal summer, as well as the intraseasonal forcing and ocean response. We show that the model reproduces reasonably well 30–90 days observed large-scale SST variations. In Sect. 4, we provide a description of observed patterns of SST and surface fluxes variations associated with monsoon active and break phases. We focus on the clear 30–90 days SST variability in four oceanic regions (northern Bay of Bengal, Oman upweling, Somalia upwelling and Southern Tip of India). In Sect. 5, we quantify the different processes responsible for SST signals in these regions. In Sect. 6, we summarize our results and discuss their implications.

2 Data, methodology and model

The approach followed in this paper is very similar to the one followed in Jayakumar et al. (2011) for the winter season. We summarize it below.

2.1 Data

The mixed layer depth and depth of the thermocline are two important parameters in the upper ocean response to forcing. We thus need to validate those fields in the model. For that purpose, we use the climatologies of mixed layer depth from de Boyer Montégut et al. (2004) and the 20°C isotherm depth derived from the World Ocean Atlas 2009 (WOA09, Locarnini et al. 2010).

We use several recent satellite datasets to describe the surface signature of the MJO in terms of SST, winds and heat fluxes. For SST, we use optimally interpolated data from the TMI instrument produced by Remote Sensing Systems, which has been extensively used to study intraseasonal SST signature of the MJO owing to its ability to "see" through clouds (Wentz et al. 2000). For winds, we use gridded estimates of 10-m winds from the QuikSCAT scatterometer produced at Centre ERS d'Archivageet de Traitement (CERSAT, Bentamy et al. 2003). Daily data for each product was averaged to a common 1° grid.

The air-sea flux product we use (TropFlux) is largely derived from the ECMWF Interim Re-Analysis (ERA-I; Dee and Uppala 2009), and is described in more detail in (Praveen Kumar et al. 2010) and Jayakumar et al. (2011). This daily heat flux dataset is available for the 1989–2009 period on a 1° regular grid. Comparison with fluxes estimated at the RAMA and TAO mooring sites (Praveen Kumar et al. 2010) shows a better performance than other available heat flux products like the NCEP (Kalnay et al. 1996) and NCEP2 re-analyses (Kanamitsu et al. 2002) or the uncorrected ERA-I fluxes, and a similar performance to the OAFLUX product (Yu and Weller 2007). We have repeated the analyses in this paper using the OAFLUX turbulent flux data (Yu and Weller 2007) and the International Satellite Cloud Climatology Project (ISCCP) radiative fluxes (Zhang et al. 2004) with similar quantitative results (not shown).

2.2 Modelling approach

Our OGCM is the Modular Ocean Model Version 4 (MOM4) set up for the Indian Ocean basin between 40°S–25°N and 30°E–120°E with 30 vertical levels. The upper ocean has 15 vertical levels within a depth of 155 m, and so the mixed layer and thermocline zones are well resolved. The zonal resolution is 1° and the meridional resolution varies from 0.33° at equator to 0.7° at 25°N and 1.5° at 40°S. Vertical mixing is based on the K-profile parameterization scheme (KPP; Large et al. 1994), with Bryan-Lewis background diffusivity (Bryan and Lewis 1979). Bottom topography is derived from the 5-min global topography ETOPO5 (Earth Topography-5 min) database. Horizontal friction is based on the shear-dependent Smagorinsky viscosity following Griffies and Hallberg (2000). Temperature and salinity at the southern and eastern boundaries are restored to monthly climatologies of Levitus (1998). Details of the model are provided in Thompson et al. (2006).

The model is initialized using temperature and salinity from Levitus (1998), and spun up for a 20-year period using climatological forcing (Large and Yeager 2004). Subsequently, it is integrated over the 1958–1995 period using the Interannual Forcing data sets from the Common Ocean-ice Reference Experiments (CORE) (Large and Yeager 2004). The control experiment (hereafter CTL) is then run for the 1996–2006 period using the same forcing

product. Air–sea fluxes are computed interactively via bulk formulae, using model SST and specified 10-m wind, air-temperature, specific-humidity, and shortwave- and long-wave-radiation fields.

We perform a series of sensitivity experiments to evaluate the importance of different physical processes on SST intraseasonal variability in the northern Indian Ocean (see Table 1). Specifically, we store the solar (shortwave) and non-solar (sensible + latent + longwave) heat flux components as well as wind stress computed by the model during the CTL, and then perform a series of sensitivity experiments with modified versions of these forcing fields. Several of the tests involve filtering to remove intraseasonal variability from the forcing fields. Toward that end, we filter the various forcing fields using a 120-day low pass filter (see Jayakumar et al. 2011 for a more extensive justification of the filtering approach).

Table 1 summarizes the experiments used in this study. The NO_ISO_STRESS experiment retains the full spectrum of heat flux forcing, but has low-passed wind stress forcing. The NO_ISO_FLX experiment still has full wind-stress forcing, but all the solar and non-solar components of the heat flux forcing are low-passed to eliminate the influence of intraseasonal flux forcing. The NO_ISO_SW experiment further attempts to isolate explicitly the effect of shortwave heat-flux variations, forcing the model with full wind stress and non-solar heat flux but filtering out intraseasonal variations of the net shortwave radiation. The NO_ISO experiment forces the model with low-passed filtered wind-stress and heat-fluxes (shortwave and net), and allows estimating the contribution from internal oceanic intraseasonal variability. All sensitivity experiments were run over 1996–2006, from the same initial condition as in the CTL experiment. We analyze the results over the 1996–2006 period.

Using the above experiments, our goal is to evaluate the contribution of various processes to the intraseasonal variability of SST,

$$SST' = SST'_\tau + SST'_Q + SST'_F + SST'_r \qquad (1)$$

where the primes indicate the intraseasonal SST variability obtained by filtering in the time domain. The first two

terms on the r.h.s. of (1) are defined by the differences $SST' = SST'_{CTL} - SST'_{NO\_ISO\_FLX}$ and $SST'_Q = SST'_{CTL} - SST'_{NO\_ISO\_FLX}$; they estimate the contribution of wind-stress and heat-flux forcing to intraseasonal SST variability, respectively. The term SST'_F, defined by $SST'_F = SST'_{NO\_ISO\_FLX}$, is the residual intraseasonal variability remaining in the NO_ISO experiment. It arises from two sources: internally generated oceanic variability, and intraseasonal freshwater forcing. The SST'_r contribution is computed as a residual, and arises mainly from nonlinearities in the ocean response. Table 3 shows that the contributions from SST'_r are small (of the order a few %) except in the Oman and northern Bay of Bengal regions where they reach ∼14 %. This contribution should be seen as an error bar on the estimation of other terms (i.e. this "error" on individual terms arises from the fact that they don't add up perfectly because of non-linearities).

One of the objectives of this paper is to provide a precise quantification of the contributions of various processes to the total intraseasonal SST variability. Toward that end, we obtain regression coefficients of the various contributions in (1) to the total SST intraseasonal variability SST'. These coefficients are computed for the entire experiment (Table 4) but also separately for each June–September season (range given in parentheses in Table 4) in order to quantitatively summarize the contribution of a specific process for each year. By construction, the coefficients for the processes in (1) sum to 1. We will give these coefficients as percentages in the paper: they always sum to 100 % but can be negative for a process that has a negative correlation to the total variability.

3 Background simulated oceanic structure and summer intraseasonal SST variability

3.1 Background oceanic structure in June–September

The depth of the thermocline and the mixed layer depth (MLD) in the NIO region are two potentially important factors controlling the amplitude of SST signature especially in the Bay of Bengal basin (Sengupta and Ravichandran 2001; Sengupta et al. 2001). Figure 1a, b shows the observed thermocline (estimated from the depth of the 20 °C isotherm, D20) and mixed layer depth (MLD) in the northern Indian Ocean during the June to September (JJAS) period. Corresponding model derived quantities for the same period are illustrated in Fig. 1c, d.

The model reproduces qualitatively the main features of the observed D20. A deep D20 (>150 m) is observed to the right of the low-level monsoon jet in the Arabian Sea, due to Ekman convergence in this region. On the other hand, there

Table 1 List of experiments used in this study

Name	Description
CTL	Full forcing
NO_ISO_FLX	Low-passed filtered shortwave and non-solar heat fluxes
NO_ISO_SW	Low passed filtered shortwave flux
NO_ISO_STRESS	Low passed filter wind stress
NO_ISO	Low passed filtered shortwave and non-solar heat fluxes, Low passed filtered wind stress

Fig. 1 June–September climatological values of depth of **a** the 20°C isotherm from WOA09 database (Locarnini et al. 2009) and **b** of the mixed layer depth (de Boyer Montégut et al. 2004). **c**, **d** The same quantities for the CTL experiment. The *black boxes* show the various regions selected in this paper: Oman (54°E–60°E, 17°N–23°N), NB°B (80°E–95°E, 15°N–23°N), Somalia (48°E–58°E, 5°N–11°N) and STI (75°E–78°E, 5°N–9°N)
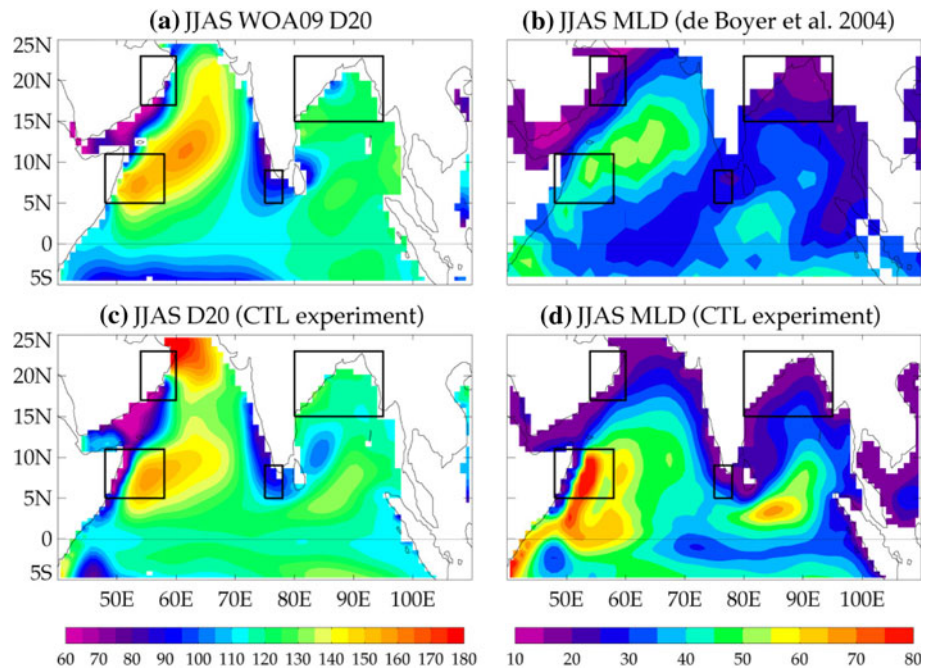
is a much shallower D20 on the left hand side of the jet and along the coast (due to the Somalia and Oman upwellings). The model also reproduces the upwelling region (thermocline shallower than 90 m) in the South-Eastern Arabian Sea and Sri Lanka Dome region (Vinayachandran and Yamagata 1998). The model also reproduces the right range of D20 depth values (100–130 m) in the Bay of Bengal. On the other hand, the model suffers from a severe bias at the northern end of the Arabian Sea, maybe due to a bad treatment of Persian Gulf and Red Sea water input.

The mixed layer of the Arabian Sea (maximum $\sim$50 m) is generally deeper compared to the Bay of Bengal (maximum $\sim$25 m), due to the stronger winds in the Arabian Sea (Prasad 2004) and stronger haline stratification in the Bay of Bengal (Shenoi et al. 2002). The model reproduces this contrast between the two basins, and the very shallow MLD observed in the northern Bay of Bengal and Northwestern Arabian Sea. Table 2 shows the model and

Table 2 Average of model and observed climatological June–September mixed layer depth and depth of the 20°C isotherm in 4 regions: OMAN (54°E–60°E, 17°N–23°N), NBOB (80°E–95°E, 15°N–23°N), Somalia (48°E–58°E, 5°N–11°N) and STI (75°E–78°E, 5°N–9°N)

Region	STI	Somalia	NBOB	Oman
Modelled/observed D20 (m)	96/94	129/145	119/120	108/97
Modelled/observed MLD (m)	25/25	56/42	22/21	18/22

The observed 20°C isotherm is obtained from WOA09 database (Locarnini et al. 2009) and the mixed layer depth from de Boyer Montégut et al. (2004)

observed climatological MLD and D20 values for the four regions of strong intraseasonal SST variability on which we will focus later in this paper (see Fig. 1 to locate these regions). The model is within 15% of observed values in all regions but the Somalia upwelling region (where the D20 seems too shallow and MLD $\sim$30% too deep). The model also seems to suffer from a too shallow MLD along the south-eastern and western coast of India. Part of the mismatch between the model and observation near the coast may also be related to observational issues. Indeed, using repeated XBT transects in the South Eastern Arabian Sea over 2002–2008 period, Gopalakrishna et al. (2009) estimated the MLD to be $\sim$20 m along the western Indian coast while estimates using the de Boyer Montégut et al. (2004) dataset is 15 m deeper.

3.2 Intraseasonal atmospheric forcing and SST signature

The model computes its own wind stress and net heat flux from specified atmospheric parameters and its own SST. Figure 2 provides a validation of the intraseasonal (30–90 days) variability of these two fields against Quickcat wind stresses and Tropflux net heat flux products.

QuikSCAT wind stresses show very clear intraseasonal variability maxima in the low-level monsoon jet region and over Bay of Bengal (Fig. 2d). Another weaker maximum is observed in the central equatorial Indian Ocean region. This structure with three maxima is very clearly related to the monsoon active and break phases, with a strong jet across the Arabian Sea, Indian subcontinent and the Bay of

Fig. 2 June–September standard deviation of 30–90 day bandpass-filtered **a** net surface flux from Tropflux dataset (Praveen Kumar et al. 2010), and **b** ERS and QuikSCAT scaterometers-derived (see text for details) wind stress module (**b**). **c**, **d** The same quantities for the CTL experiment
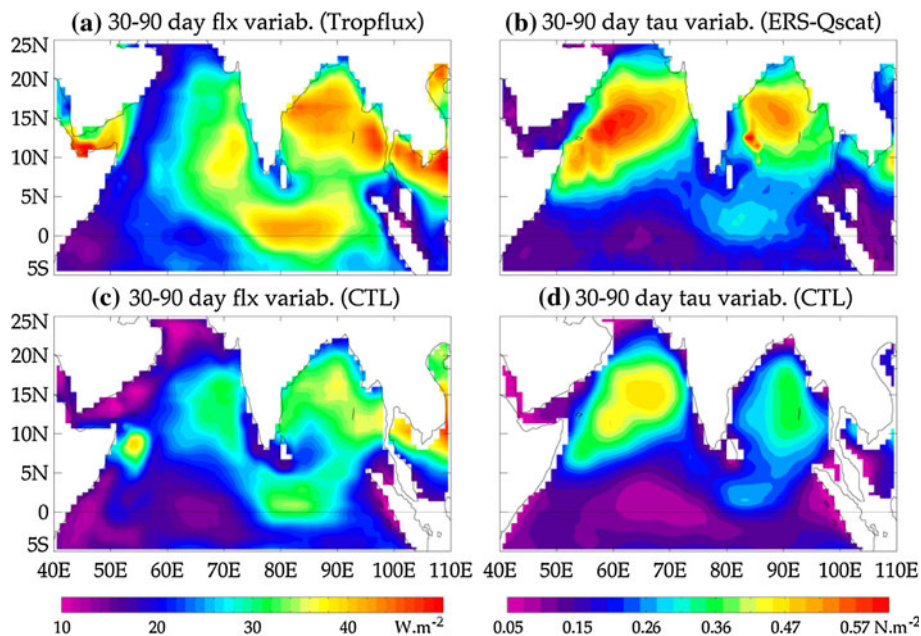
Bengal during active phases; and a jet that is deflected south and is located above the equatorial Indian Ocean during break phases (e.g. Joseph and Sijikumar 2004). The CORE wind forcing reproduces this spatial structure neatly, but with a ∼30% underestimation of the intraseasonal variability. CORE wind speed is based on NCEP re-analysis (Kalnay et al. 1996), which has a more pronounced weak bias at high wind speed (Smith et al. 2001). The CORE wind speed correction (a 5–10% increase in the northern Indian Ocean) is done on an annual basis and probably underestimates intense winds during the southwest monsoon.

The heat flux variability reproduces this 3-maxima structure east of ∼60°E. The absence of strong net heat flux perturbation in the western Arabian Sea has two main causes. First, the deep convective perturbation is largely confined to the region east of ∼60°E, thereby having a maximum shortwave radiation perturbation there. Second, the SST is much colder in the western Arabian Sea due to the Somalia and Oman upwellings, resulting in a smaller latent heat flux release by the surface wind intraseasonal perturbation. The model forcing also reproduces quite well the spatial pattern of these heat flux perturbations, although again with a smaller amplitude (∼20% underestimation). This underestimation is largely accounted by latent heat fluxes, and is linked to the wind bias mentioned above. The model however, tends to overestimate the intraseasonal heat flux perturbations over the Somalia upwelling.

Jayakumar et al. (2011) showed the model ability in reproducing the intraseasonal SST variability in the 5–10°S band of the Indian Ocean during the boreal winter. Figure 3 shows the standard deviation of 30-90 day filtered TMI and

CTL experiment SST during summer (June to September). The model captures the spatial patterns of maximum intraseasonal SST variability reasonably well, but underestimates the amplitude by a factor two in the Somalia and Oman upwelling regions. The analysis of Fig. 3 retains all spatial scales contributing to 30–90 days variability of SST. This includes large-scale variability associated with atmospheric intraseasonal variability, but also the energetic
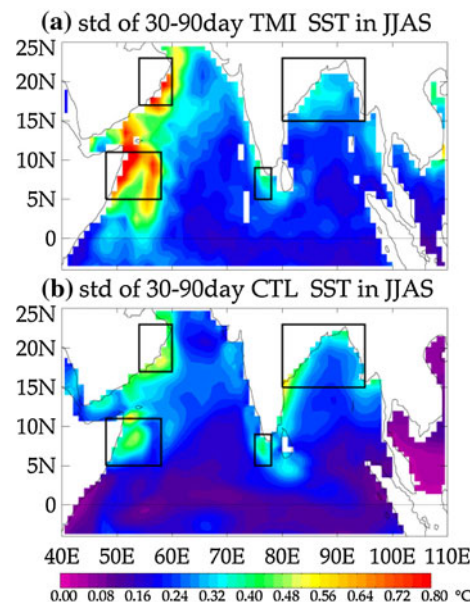

Fig. 3 Standard deviation of 30–90 day band passed 1998–2006 SST during JJAS (°C) for **a** TMI SST observation and **b** CTL experiment. The *black boxes* show the various regions selected in this paper: Oman (54°E–60°E, 17°N–23°N), NBOB (80°E–95°E, 15°N–23°N), Somalia (48°E–58°E, 5°N–11°N) and STI (75°E–78°E, 5°N–9°N)

meso-scale eddies in the Somalia and Oman upwellings (Brandt et al. 2003) and in the Bay of Bengal (Gopalan et al. 2000). The spatial resolution of our model ($\sim$1°) does not allow resolving meso-scale variability, which may explain the mismatch between Fig. 3a, b. Also note that the model tends to overestimate SST intraseasonal variability along the east coast of India: this is probably due to the too shallow MLD in this region (see Figs. 1b, d), as we will demonstrate in Sect. 5.

The frames in Fig. 3 indicate the regions of local maxima in intraseasonal SST variability, which will be used later in this paper. These regions agree well with the regions of coherent SST response to large–scale intraseasonal perturbations of convection and wind during summer discussed in Duvel and Vialard (2007). We will name these regions STI (Southern Tip of India, 75–78°E, 5–9°N), SOMALIA (Somalia upwelling, 48–58°E, 5–11°N), NBOB (northern Bay of Bengal, 80–95°E, 15–23°N) and OMAN (Oman Upwelling, 75–78°E, 17–23°N) hereafter. Figure 4 shows comparison of the average 30–90 days filtered SST in these regions. The smallest of these regions is $\sim$900 km by $\sim$550 km. The typical diameter of largest eddies in the northern Indian Ocean is about 150–200 km (Chelton et al. 2007) The smallest of our averaging regions has hence typically 16 times the area of a large eddy, and averaging over such a region will largely filter out the effects of meso-scale variability. The average model 30–90 days variability over the STI, SOMALIA, NBOB and OMAN regions (Fig. 4) has amplitude ratios to observations of 1.1, 0.74, 0.87 and 0.8, respectively. The phase agreement between the model and observed average intraseasonal SST is also good with correlations between 0.74 and 0.86. The model is hence reasonably successful to reproduce the large-scale SST variations in those regions, despite its strong underestimation of meso-scale variability (Fig. 3).

4 Observed surface signature of the summer intraseasonal oscillations

In this section, we will use surface temperature, wind and heat fluxes derived from observations to quantify the surface signature of the summer intra-seasonal oscillation.

4.1 Large scale patterns

A simple index of active and break phases of the monsoon can be constructed by taking the difference between Bay of Bengal (70°E–95°E, 10°N–20°N) and equatorial Indian Ocean (70°E–95°E, 5°S–5°N) 30-90 day filtered outgoing longwave radiation (e.g. Goswami 2005). Figure 5 shows the lag regression of SST, QuikSCAT surface wind and Tropflux heat fluxes to this normalized index for JJAS. A

very similar heat flux pattern is obtained when using the OAFLUX (Yu and Weller 2007) and ISCCP (Zhang et al. 2004) products (not shown).

The resulting wind pattern is characteristic of an active-break cycle of the summer monsoon (e.g. Goswami 2005, Joseph and Sijikumar 2004). The wind anomaly at lags −20 and 20 show an increased monsoon flow. On the other hand, the wind anomaly at lag 0 is characteristic of a break phase, with decreased wind over the northern Indian Ocean and the monsoon jet deflected around the southern tip of India, and blowing along the equator.

The strongest surface flux perturbations are $\sim$20–30 W m^{-2} and are mostly located in the Eastern Indian Ocean (i.e. east of 65°E, cf. discussion in 3.2). These flux perturbations follow the northward movement of the active break cycle, with negative heat flux perturbations associated with increased convection and surface wind during the active phase. Figure 5 shows the Bay of Bengal SST signal, which has been discussed in several studies (e.g. Sengupta and Ravichandran 2001; Sengupta et al. 2001; Vecchi and Harrison 2002; Waliser et al. 2004; Duncan and Han 2009), but also clear signals in the Arabian Sea which were pointed out in few previous studies (Duvel and Vialard 2007; Roxy and Tanimoto 2007; Wang et al. 2006), but never discussed in detail.

Figure 6 shows that the SST signals in the Arabian Sea are of roughly similar amplitude than those in the Bay of Bengal. Warm SST anomalies first appears near the southern tip of India $\sim$ 8 days before a break phase (Figs. 5b, 6), then in the Somalia upwelling region $\sim$2 days after the break (Figs. 5c, 6). The warming in the northern Bay of Bengal follows the break by $\sim$11 days while the warming in the Oman upwelling appears last, $\sim$15 days after the break phase. Figure 5 shows a clear northward propagation of SST anomalies along the Oman coast, as well as some weaker sign of northward propagation of SST anomalies along Somalia.

Figure 6b shows the correlation coefficient (rather than the regression in Fig. 6a) of averaged intraseasonal SST in each region with the active/break index. This shows that SST in NBOB has the strongest association with active/ breaks (correlation $\sim$0.55), followed by OMAN (correlation $\sim$0.4). The SOMALIA and STI regions have a much weaker association with the active/break index. In order to investigate whether SST intraseasonal variability in those regions is due to a different mechanism, we repeated the analysis of Fig. 5, but using a regression index based on the 30–90 days average SST in each region. Figure 7 shows the patterns associated with each of the regions (with selected lags in order to correspond to lag 0 of Fig. 5). In general, all patterns are quite similar, and reminiscent of the active-break cycle. Most of the SST large-scale intraseasonal variability in the 4 boxes is hence associated with large scale atmospheric intraseasonal variability linked to

Fig. 4 Average 30–90 days band passed SST for TMI SST observation (*red*) and CTL experiment (*black*) for the four regions displayed in Fig. 3: **a** Oman, **b** NBOB, **c** Somalia and **d** STI. The correlation coefficient (*r*) and the standard deviation (std) of observations (obs) and the model (mod) for the JJAS period are indicated in each *panel*
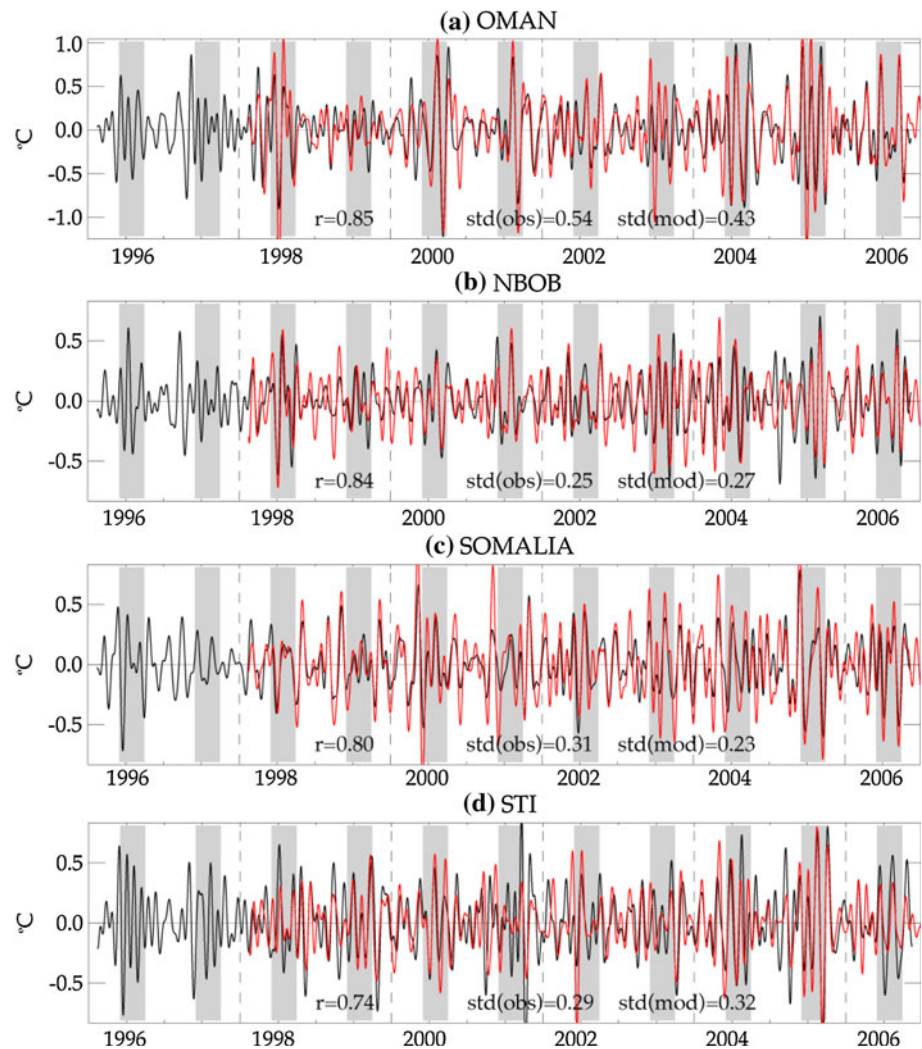
active and break monsoon phase. Active and break phases; however, do have a significant event-to-event variability in the details of their spatial patterns (see e.g. Duvel and Vialard 2007). When this pattern is, for example, much more shifted toward the Arabian Sea, as in Fig. 7d, the perturbation over the Somalia upwelling is larger and hence the SST intraseasonal response. However, in general, most consistent responses to active and break events occur over the NBOB and OMAN regions (Fig. 6b).

4.2 Mechanisms of the oceanic response

Figures 8 and 9 have been obtained by regression to the JJAS normalised 30–90 days SST averaged over the four regions. This allows isolating the typical atmospheric and surface heat flux perturbations associated with SST intraseasonal variability in each region, in order to diagnose its mechanisms.

The OMAN region experiences the strongest box-average SST intraseasonal variability (~ 0.5°C) while typical variability in other boxes is rather ~ 0.3°C. As already pointed out, the convective perturbations are strongest over the eastern Arabian Sea and Bay of Bengal (e.g. Joseph and Sijikumar 2004). The intraseasonal wind speed perturbations range from ~ 0.5 to 1 m/s with largest wind speed perturbations over the Bay of Bengal. The net heat flux perturbations are ~ 25 W m^{-2} over NBOB, about ~ 17 W m^{-2} over STI, and ~ 10 W m^{-2} over the Arabian Sea. The heat flux perturbations are due to shortwave radiations (~ 60%) and latent heat fluxes (~ 40%) over NBOB, with compensation between sensible and longwave fluxes. The shortwave contribution is slightly larger (~ 70%) over the STI region.

The SST perturbations in the Arabian Sea are of the same order or larger than those in the Bay of Bengal. On the other hand, the flux perturbations tend to be significantly smaller over the Arabian Sea than over the Bay of Bengal. This suggests that heat flux forcing probably plays a smaller role in driving intraseasonal SST variability over the Arabian Sea compared to the Bay of Bengal. In order to
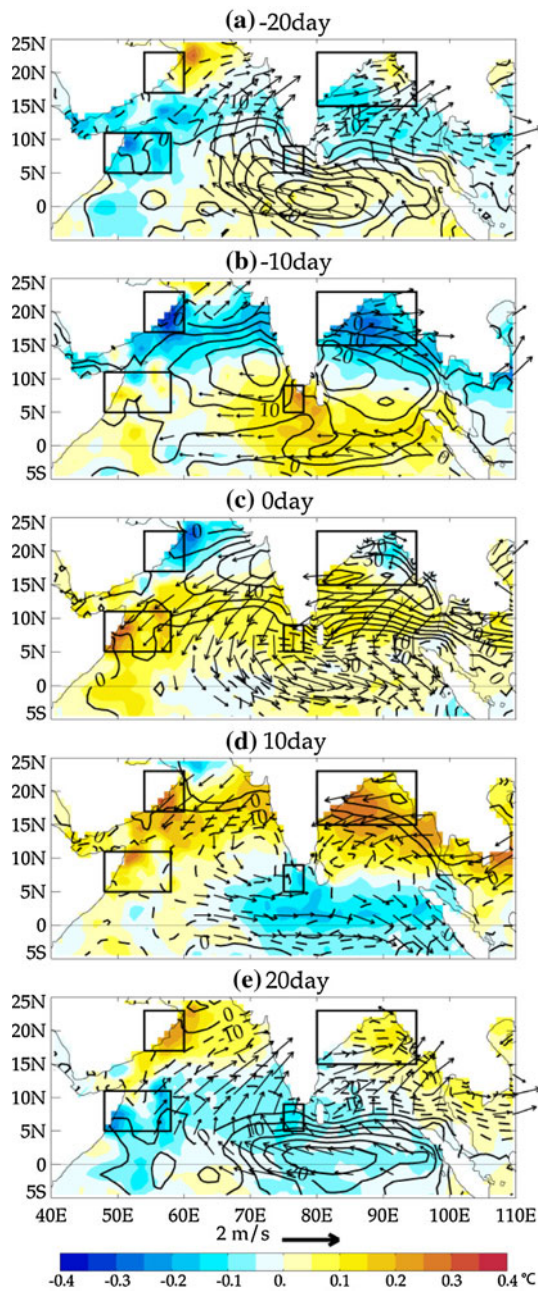
Fig. 5 Regression of 30–90 days June–September TMI SST (°C, colors), QuikSCAT wind (m s^{-1}, vectors) and Tropflux surface net heat flux (W m^{-2}, contours) to a normalized active/break monsoon index (see text for details) at **a** 20 days before, **b** 10 days before, **c** 0 day before, **d** 10 days after and **e** 20 days after a break monsoon phase
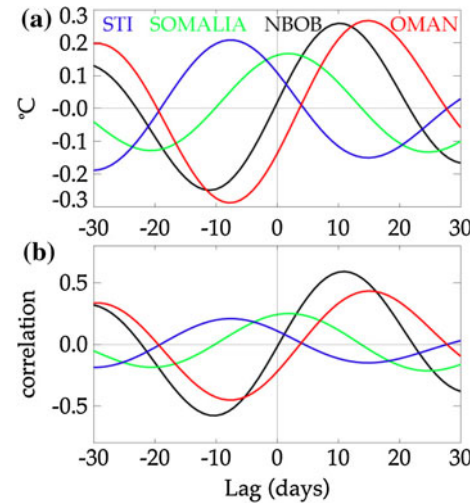

Fig. 6 a Average of the regressed SST shown in Fig. 5 over the four reference regions: Oman (*red*), NBOB (*black*), Somalia (*green*) and STI (*blue*). **b** Average of the corresponding correlation (of correlation of SST to active/break phase index). The maximum SST perturbation is at lag −8, 2, 11 and 15 days before/after a break phase for STI, Somalia, NBOB and Oman, respectively

climatological mixed layer depth from de Boyer Montégut et al. (2004). We integrate Eq. (2) using the daily Tropflux net heat flux Q_0 and then evaluation the intraseasonal component by 30–90 days filtering. The SST is then compared to the observed SST intraseasonal variability (Fig. 10b). The intraseasonal SST obtained from (1) will compare favourably to observed SST in regions where: (1) heat flux forcing dominates the heat budget, (2) mixed layer depth (h) variations do not contribute strongly to the SST variability and (3) observed estimates of net heat flux (Q_0) intraseasonal variations are accurate.

Figure 10a shows the standard deviation of the 30–90 SST variability obtained from the slab ocean approach (the colour scale is different from the one in Fig. 3a). This figure reflects partly the distribution of the net heat flux variability from Fig. 2a, with a modulation from the mixed layer depth (Fig. 1b). The shallow mixed layers and strong net heat flux intraseasonal variability combine to produce a SST intraseasonal variability maximum in the northern Bay of Bengal while deeper mixed layer damps the SST response in the equatorial Indian Ocean and Arabian Sea. Figure 10b shows that the slab ocean approach is performing well in the northern Bay of Bengal. The NBOB average slab ocean SST variability has a regression coefficient of 0.82 to the TMI 30–90 days SST in the same region (Table 3). This confirms the findings of previous studies (e.g. Sengupta and Ravichandran 2001; Duncan and Han 2009): heat flux forcing appears to be the dominant process in the northern Bay of Bengal. The slab ocean approach also explains ∼40% of the observed 30–90 days SST variability in the STI region (Table 3), but performs

investigate that more thoroughly, we have used a slab-ocean mixed layer approach:

$$\frac{\partial T}{\partial t} = \frac{Q_0}{\rho c_p h} \tag{2}$$

where Q_0 is the net heat flux at the air-sea interface, ρc_p is the heat capacity of seawater, and h is the June–September
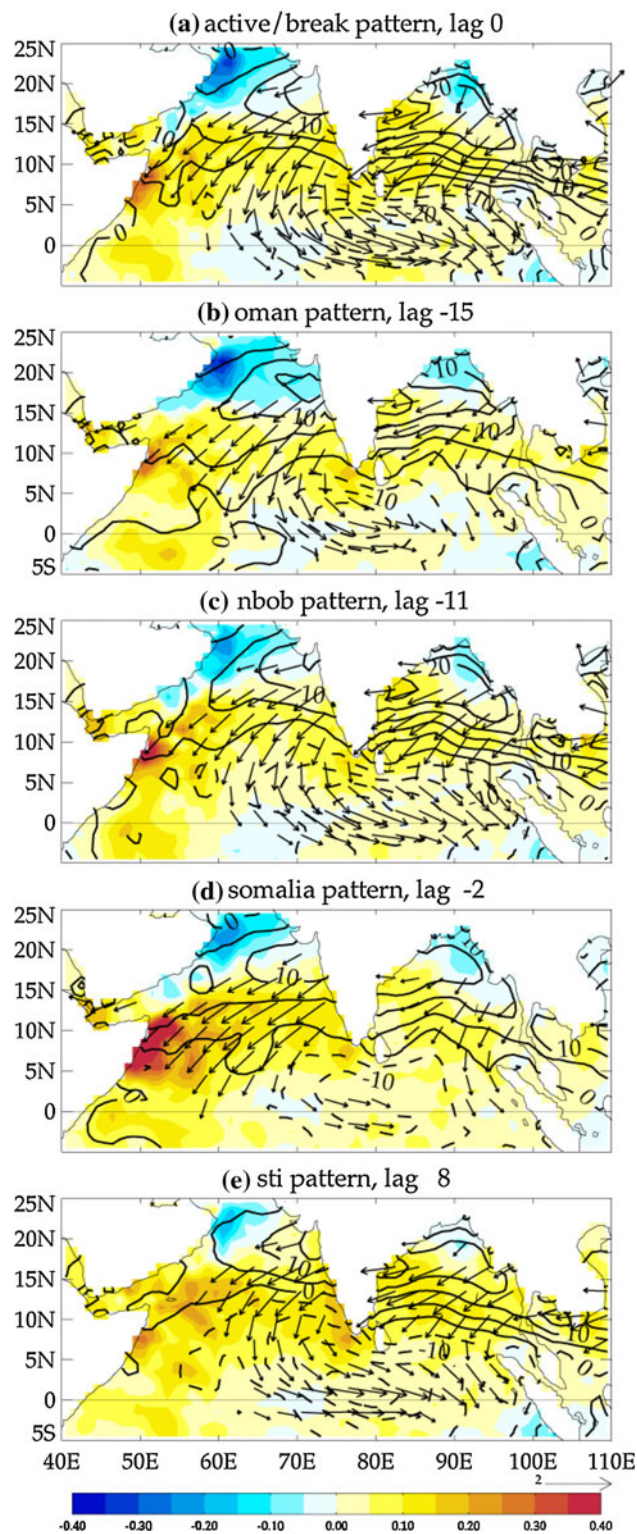
Fig. 7 Comparison of the wind stress, net flux and SST patterns obtained from regression to **a** active-break index (similar to **c** in Fig. 5) and SST indices from the 4 regions (**b–e**). The lags have been chosen in order to be able to compare **a–e**
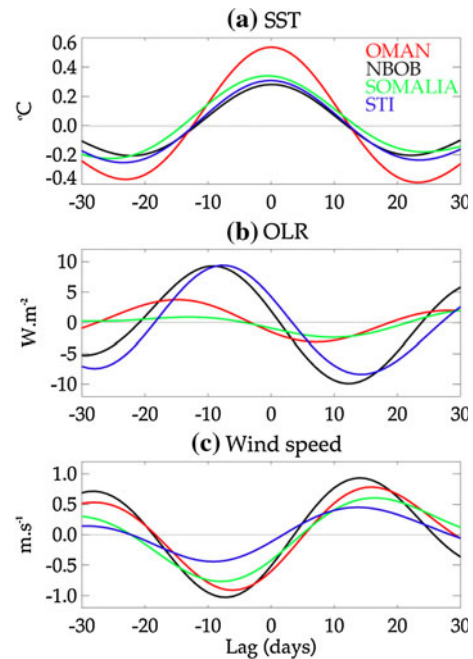

Fig. 8 June–September intraseasonal (30–90 days), **a** TMI SST, **b** NOAA OLR and **c** QuikSCAT wind speed associated with typical SST perturbations in the four reference regions: Oman (*red*), NBOB (*black*), Somalia (*green*) and STI (*blue*). Each 30–90 days filtered variable is averaged over the region and regressed to the normalized 30–90 days SST over the same region

poorly over the other regions. This is an additional suggestion that oceanic processes contribute significantly to SST intraseasonal variability in the Arabian Sea.

5 Processes of the modelled 30–90 days summer intraseasonal SST variability

We saw in Sect. 3 that the model reasonably reproduces the large-scale 30–90 days SST response in the four regions considered in this study. In this section, we hence use the model to evaluate the respective contributions of surface heat flux and wind stress forcing to the intraseasonal SST variability in the northern Indian Ocean.

In Fig. 11, we have repeated the slab-ocean approach of Fig. 10, but now using Q_0 and climatological June–September h from the model. First, there is an overall striking similarity between Figs. 10a, b and 11a, b. Some differences however, allow us understanding some of the model biases. For example, the model tends to overestimate the 30–90 days SST variability along the east coast of India (Fig. 3), while the spatial distribution of forcing is reasonable in this region (Fig. 2). Figure 11a shows that the shallow MLD along the east coast of India compared to
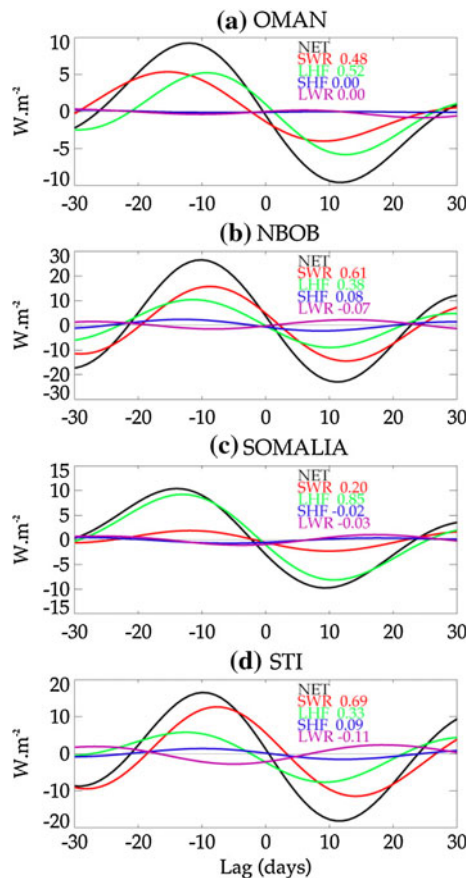
Fig. 9 June–September intraseasonal (30–90 days) net heat flux (*black*) perturbation and its four components (shortwave radiation in *red*, latent heat flux in *green*, sensible heat flux in *blue* and longwave radiation in *purple*) regressed to normalized average 30–90 days SST for: **a** Oman, **b** NBOB, **c** Somalia and **d** STI

Fig. 10 a Standard deviation of June–September intraseasonal (30–90 days) SST variability estimated from a slab-ocean approach in observations (using climatological mixed layer depth as in Fig. 1b and Tropflux net heat fluxes). **b** Regression of this SST to 30–90 days observed (TMI) SST

Table 3 Regression coefficient of the regional average 30–90 days SST obtained from the slab ocean approach with Tropflux fluxes (see text for details) to the regional average 30–90 days observed SST

Region	STI	Somalia	NBOB	Oman
Regression coefficient (obs)	0.38	0.17	0.82	0.18
Regression coefficient (model)	0.24	0.27	0.71	0.06

The second line shows the same diagnostic, but from modelled outputs

observations (Fig. 1) results in an amplification of the atmospheric heat flux forcing, and overestimated 30–90 days SST variability in this region. Apart from this feature, Fig. 11 confirms that the maxima of 30–90 days SST variability in the northern Bay of Bengal is largely explained by a slab-ocean response to atmospheric forcing. On the other hand, intraseasonal atmospheric forcing explains a small fraction of the SST intraseasonal variability in the Arabian Sea regions. This is quantitatively confirmed by Table 3, which shows that a simple slab ocean explains more than 70% of the 30–90 days SST variability in the NBOB region, while it always explains less than 40% of it in both model and observations in the three Arabian Sea boxes.

The series of sensitivity experiments described in Sect. 2 allow us to evaluate the respective contributions of heat fluxes, wind stress, internal variability and other non-linearities in the 30–90 days SST variability in the model. Figure 12 shows a map of these contributions, while Table 4 provides the various contributions to the average intraseasonal SST variability in each region.
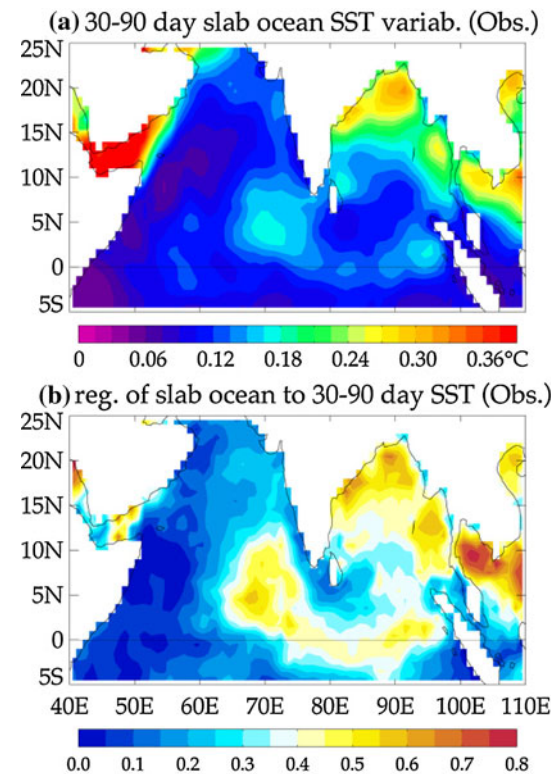
In the northern Bay of Bengal, most of the SST 30–90 days variability (Fig. 12a) is due to heat flux forcing (Fig. 12b, Table 4: 89%), with shortwave radiations contributing significantly (Fig. 12c). Wind stress also contributes positively, but to a much smaller extent (Fig. 12d, 26%). Internal variability does not play a big role in the northern Bay of Bengal (Fig. 12e, −2%). On the other hand, non-linearities contribute negatively (Fig. 12d, −13%). This last feature can probably be understood in the following way. For example, during an active phase, there is both an increase of mixing and heat losses at the sea surface. The increased mixing enhances the mixed layer depth, and hence "dilutes" the negative surface heat flux
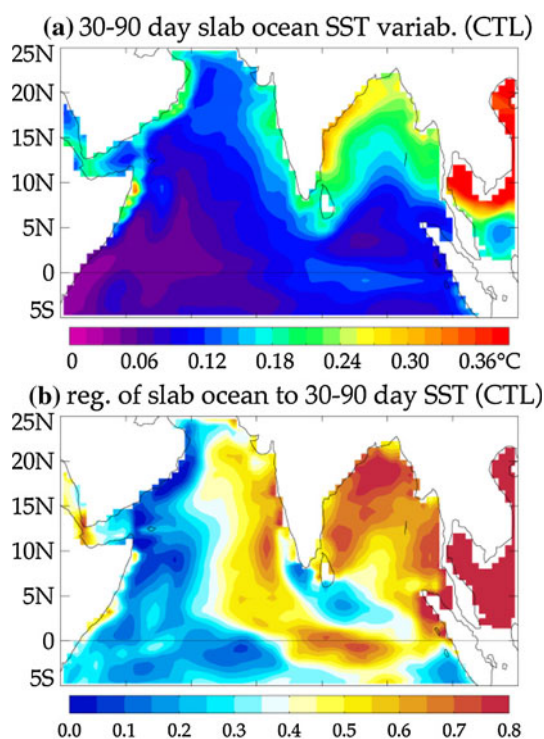
Fig. 11 **a**, **b** Similar to Fig. 9, but computed from CTL experiment outputs

perturbation (i.e. non-linearities tend to diminish the overall SST cooling).

In the Arabian Sea, in general, the model confirms the tendency suggested by observations: oceanic dynamical processes generally dominate the SST intraseasonal variability, while the heat flux forcing tends to play a secondary role (Fig. 12). In the STI region, the model suggests that the SST intraseasonal variability is almost entirely driven by wind stress variations (Fig. 12d, Table 4: 95%) with negligible role from other processes. In the OMAN region, wind stress is responsible for most of the SST 30–90 days variability (104%, Table 4). Heat fluxes contribute negatively to the 30–90 days SST variability (−15%). This could be the sign of a negative feedback of atmospheric heat fluxes on intraseasonal SST variations in this region.

The Somalia upwelling region is known as a region of strong meso-scale variability. Although the 1° resolution does not allow the model to resolve this variability properly, Fig. 12e shows that this is the only region where internal variability contributes significantly to the 30–90 days SST variability in the model. However, while this contribution is not negligible at the model resolution (it contributes top 32% of the variability, Table 5), it is not coherent in space and disappears when the SST is averaged over the whole Somalia region (3% Table 5). At the scale of the Somalia box, non-linearities and internal variability

are negligible, and the SST 30–90 days variability is mostly driven by wind-stress variations (71%), with a non-negligible contribution from heat fluxes (22%).

Table 4 also provides an idea of the year-to-year variations of each process to the 30–90 days SST variations. Heat fluxes are always the dominant process in the NBOB region, although wind stress can occasionally contribute to up to 40% of the SST variations. Wind stress is also quite systematically the dominant process over the Oman upwelling, although other processes can occasionally contribute to up to 45% of the SST variations. Wind stress also dominates the STI and SOMALIA regions, but with more significant variations of the contributions from other processes.

To summarize this section, the model shows that SST intraseasonal variability is largely due to heat fluxes in the northern Bay of Bengal and to wind-stress fluctuations in the 3 upwelling regions of the Arabian Sea (Oman, Somalia and Southern Tip of India). Eddies contribute to intraseasonal SST variability at small scale in the Somalia upwelling region, but their contribution is not coherent in space and vanished at the spatial scale of the upwelling itself.

6 Summary and discussion

6.1 Summary

In this paper, we have used a combination of observations and modeling to understand the main factors that drive intra-seasonal SST variability in the northern Indian Ocean during boreal summer. Northward propagating deep-atmospheric convective perturbations are associated with large-scale intraseasonal SST variability in the northern Bay of Bengal, but also in the Somali and Oman upwelling regions and close to the Southern tip of India. Concurrent with the northward propagation of atmospheric intraseasonal oscillations, the SST variations appear first at the southern tip of India (day 0), in the Somali upwelling (day 10), northern Bay of Bengal (day 19) and finally Oman upwelling (day 23), as the atmospheric intraseasonal oscillation moves northward. While the variability in the Bay of Bengal has been described extensively in other studies, this is to our knowledge the first study that details variations of the Arabian Sea associated with monsoon active and break phases.

While the typical amplitude of observed SST perturbations is about the same in these three regions (~ 0.4°C), the surface heat flux perturbations are significantly larger in the northern Bay of Bengal (~ 25 W m^{-2}) than in the Arabian Sea (less than 10 W m^{-2} in the western Arabian Sea, about 18 W m^{-2} near southern tip of India). Temporal

Fig. 12 a Standard deviation of JJAS 30–90 band-passed SST for the 1996–2006 period in CTL experiment and contributions from **b** intraseasonal heat fluxes, **c** intraseasonal shortwave fluxes, **d** intraseasonal wind stress, **e** internal variability and **f** residual. See text for details on how each component is evaluated. The contributions in **b–f** are computed as the correlation to the total SST variability, multiplied by its standard deviation (as in **a**). With such a normalization, **b**, **d**, **e** and **f** add up to **a**
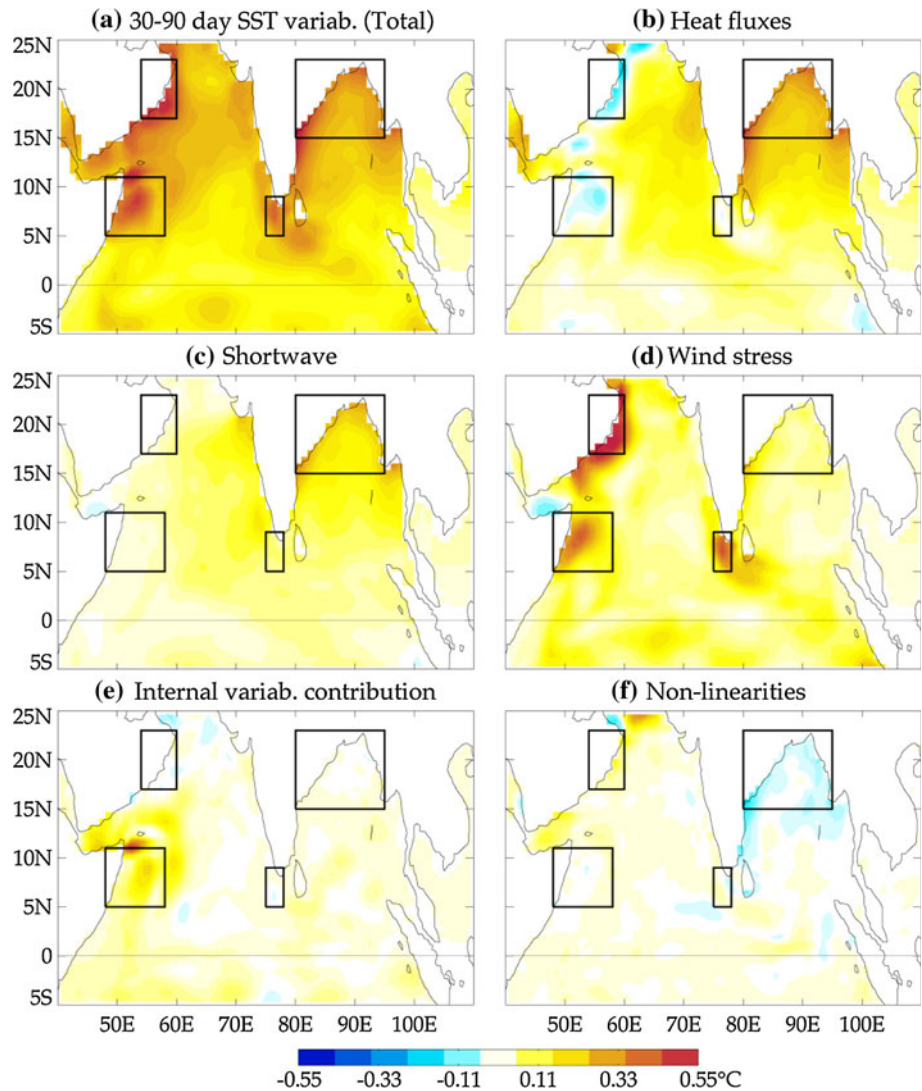

Table 4 Regression coefficient of the 30–90 days average SST variability associated with heat flux forcing, wind stress forcing, internal variability and residual over each region with the total 30–90 days variability in the CTL experiment

Contribution of each process	STI	Somalia	NBOB	Oman
Heat flux	0.04 (−0.25–0.56)	0.22 (0.01–0.35)	0.89 (0.83–1.01)	−0.15 (−057–0.21)
Wind stress	0.95 (0.36–1.16)	0.71 (0.43–1.04)	0.26 (−0.10–0.41)	1.04 (0.85–1.25)
Internal variability	−0.03 (−0.16–0.07)	0.03 (−0.23–0.45)	−0.02 (−0.06–0.04)	−0.03 (−0.14–0.06)
Non linearities	0.04 (−0.12–0.22)	0.04 (−0.05–0.15)	−0.13 (−0.15–0.04)	0.14 (−0.17–0.22)
Heat flux + wind stress	0.99 (0.80–1.13)	0.93 (0.56–1.25)	1.15 (0.91–1.29)	0.89 (0.67–1.25)

Note that by construction, the sum of the contribution of residual, error (uncertainties in the estimation of each processes due to non-linearities), wind stress and heat flux regression coefficients is equal to 1 (i.e. those can be seen as estimates of the percentage of variability explained by a certain process). The numbers in parentheses show the range of these values for individual years from 1996 to 2006

integration of surface heat fluxes over a climatological mixed layer depth is reasonably successful in capturing the SST variability in the northern Bay of Bengal, in both model and observations. They however, fail to do so in the three regions of the Arabian Sea. Sensitivity experiments with the OGCM confirm the dominant role of air-sea fluxes ($\sim$90%) in the northern Bay of Bengal, and show that wind-stress intraseasonal variations are the primary factor that drives the 30–90 days SST variability in the three regions of the Arabian Sea (>70%). The relative contributions of various processes to SST intraseasonal variability however, has greater year to year variability in the

Table 5 Comparison of the relative influence of various processes in the Somalia box, given as a regression coefficient, at large-scale (i.e. box average SST) and model resolution

Contribution of each process	Large-scale	Model resolution
Heat Flux	0.22	−0.01
Wind stress	0.71	0.69
Internal variability	0.03	0.32
Error	0.04	0.00
Heat flux + wind stress	0.93	0.68

The first column is a column 2 in Table 2 (computed from the box-average SST) whereas the second column is the box average of the pointwise regression coefficients for each process. The lines of the table are identical to Table 2

Somalia and Southern Tip of India regions, while wind stress and heat flux variation tend to always be the dominant process in the Oman upwelling and northern Bay of Bengal, respectively.

6.2 Discussion

The coarse resolution of our model (1°) is of course a strong caveat to our study. The model is not able to reproduce the strong meso-scale variability that is observed in the Somalia and Oman upwelling regions (Fig. 3). Our assumption here is that, in parallel to this small scale (<100 km) SST variability associated with eddies, there are larger-scale variations associated with variations of the intensity of the whole upwelling systems and of air-sea fluxes, and that the model is able to capture these variations. We chose averaging regions based on Fig. 3, with a size typical of the SST response to monsoon active and break phases, in both the model and observations. The smallest of these regions is ~900 km by ~550 km. The typical diameter of largest eddies in the northern Indian Ocean is about 150–200 km (Chelton et al. 2007). The smallest of our averaging regions has hence typically 16 times the area of a large eddy, and averaging over such a region will largely filter out the effects of meso-scale variability. When averaged over such a region, the model SST is indeed in reasonable agreement with the observed one (Fig. 4, with correlations above 0.74 and an amplitude within ± 25% of the observed one). Our assumption that the model is able to capture the large-scale variations of SST associated with active and break phases of the monsoon, despite a strong underestimation of meso-scale variability hence seems reasonable. The eddy variability in this region might however be itself modulated by the monsoon intensity (Brandt et al. 2003), and the mean state in the region is intricately linked to the presence of strong lateral mixing induced by active meso-scale variability in the region. Another limitation of this study is that the

surface forcing intraseasonal variability itself seems to be underestimated in this study (by ~30% for wind stress and ~20% for heat fluxes). The results of the current study will hence have to be confirmed with a higher-resolution model with more accurate forcing.

Another strong limitation of this study is the forced framework. First, although the model does not have explicit relaxation to observed SST, but rather computes its own air-sea fluxes through bulk formulae, this approach is not fully consistent as pointed out by de Boyer Montégut et al. (2007) over the same region at interannual timescales. In the real atmosphere, the air temperature and humidity adjusts to the SST after a few days due to the stronger heat capacity of the ocean mixed layer. In our experiments, air temperature and humidity are specified, which is almost equivalent to a relaxation to the air temperature as pointed out in de Boyer Montégut et al. (2007). Using a coupled model would allow to overcome this difficulty and have more coherent upper ocean heat budgets (but at the expense of being able to compare modelled events with observed one). In addition to that, several studies have pointed out the strong air-sea coupling that exists at small spatial scales over the Arabian Sea upwelling regions (e.g. Vecchi et al. 2004) with potential influence on the mean state of the ocean in the region (Seo et al. 2008).

There have been several other studies that diagnosed processes responsible for SST intraseasonal variations during summer over the Bay of Bengal. Our study suggests that air-sea fluxes is responsible of ~90% of the SST variations over the Bay of Bengal, and that this number does not vary strongly from year to year. While observational studies generally do not quantify exactly the contribution of fluxes against other processes, most of them attributed a large part of the SST large-scale variations in the northern Bay of Bengal to intraseasonal air-sea fluxes (Sengupta and Ravichandran 2001, Duvel and Vialard 2007). The Duncan and Han (2009) model study also suggest that air-sea fluxes (and more specifically latent heat flux variations) dominate SST variability in the Bay of Bengal, but the region they selected is not in the area of the maximum SST intraseaonal variability. Several other modelling studies (Fu et al. 2003, Waliser et al. 2004, Bellon et al. 2008), suggest that air-sea flux is the dominant process that drives intraseasonal variability in the northern Bay of Bengal, but also find a non-negligible contribution of oceanic processes (mixing, Ekman pumping, vertical advection). In comparison, we find a ~26% contribution of oceanic processes: although this number is non-negligible, this contribution varies a lot from year to year and is hence probably only marginally statistically significantly associated with monsoon active and break phases. Overall, we feel that there is a reasonable consensus in designating

air-sea fluxes as the main driver of large-scale intraseasonal SST variations in the northern Bay of Bengal.

In comparison with the Bay of Bengal, there have been only a few observational studies of SST anomalies associated with monsoon active and break phases over the Arabian Sea (Roxy and Tanimoto 2007, Joseph and Sabin 2008) and none of them discussed the oceanic processes associated with those SST variations in detail. The only modelling study that addressed summertime intraseasonal SST variations in the Arabian Sea in detail is Duncan and Han (2009), but they did not select the regions of maximum SST variations (i.e. the Oman, Somalia and Southern Tip of India upwelling regions) but rather a region in the Central, Southern Arabian Sea (their Fig. 6). In this region, they find an equivalent influence of intraseasonal variations of latent heat flux (changes in wind speed) and of wind stress, i.e. they find a comparatively larger effect of wind stress than in the Bay of Bengal. There is thus a qualitative agreement between our results and theirs in designing wind stress variations as a more important factor in driving SST variations in the Arabian Sea than in the Bay of Bengal.

Our paper suggests that wind-stress intraseasonal variations are much more important in driving SST response to the monsoon active and break phases over the Arabian Sea than over the Bay of Bengal. This is suggested by both applying a slab-layer integration of observed fluxes and by sensitivity experiments with an OGCM. We did not, however, identify specifically the ocean processes associated with those intraseasonal wind-stress variations. In principle, those will drive upwelling, both through Ekman pumping and coastal upwelling (when the wind stress perturbation is along the coast), i.e. changes in SST through vertical advection. This will also induces variations in mixing and entrainment by injecting turbulence into the oceanic mixed layer. The wind-stress intraseaonal perturbations may also drive an upper ocean current response and hence an advection intraseasonal perturbation. As mentioned above, the intraseasonal wind stress perturbations can also modulate the eddy activity in the upwelling region (Brandt et al. 2003), and hence the "lateral mixing" associated with those eddies. A detailed analysis of the relative contributions of these oceanic processes would be of interest in a future study with a higher lateral resolution and improved surface forcing (either forced or coupled).

References

Annamalai H, Slingo JM (2001) Active/break cycles: diagnosis of the intraseasonal variability of the Asian summer monsoon. Clim Dyn 18:85–102

Ajaya Mohan RS, Goswami BN (2003) Potential predictability of the Asian summer monsoon on monthly and seasonal time scales. Met Atmos Phys, doi:10.1007/s00703-002-0576-4

Bellon G, Sobel AH, Vialard J (2008) Ocean-atmosphere coupling in the monsoon intraseasonal oscillation: a simple model study. J Clim 21:5254–5270

Bentamy A, Katsaros KB, Alberto M, Drennan WM, Forde EB, Roquet H (2003) Satellite estimates of wind speed and latent heat flux over the global oceans. J Clim 16:637–656

Brandt P, Dengler M, Rubino A, Quadfasel D, Schott F (2003) Intraseasonal variability in the southwestern Arabian Sea and its relation to the seasonal circulation. Deep Sea Res II 50:2129–2142

Bryan K, Lewis LJ (1979) A water mass model of the world ocean. J Geophys Res 84:2502–2517

Chatterjee P, Goswami BN (2004) Structure, genesis and scale selection of the tropical quasi-biweekly mode. Q J R Meteorol Soc 130:1171–1194

Chelton DB, Schlax MG, Samelson RM, de Szoeke RA (2007) Global observations of large oceanic eddies. Geophys Res Lett 34:L15606. doi:10.1029/2007GL030812

de Boyer Montégut C, Madec G, Fischer AS, Lazar A, Iudicone D (2004) Mixed layer depth over the global ocean: an examination of profile data and a profile-based climatology. J Geophys Res 109:C12003. doi:10.1029/2004JC002378

de Boyer Montégut C, Vialard J, Shenoi SSC, Shankar D, Durand F, Ethé C, Madec G (2007) Simulated seasonal and interannual variability of mixed layer heat budget in the northern Indian Ocean. J Clim 20:3249–3268

Dee DP, Uppala S (2009) Variational bias correction of satellite radiance data in the ERA-Interim reanalysis. Q J R Meteorol Soc 135:1830–1841

Duncan B, Han W (2009) Indian Ocean intraseasonal sea surface temperature variability during boreal summer: Madden-Julian Oscillation versus submonthly forcing and processes. J Geophys Res 114:C05002. doi:10.1029/2008JC004958

Duvel JP, Vialard J (2007) Indo-Pacific sea surface temperature perturbations associated with intraseasonal oscillations of the tropical convection. J Clim 20:3056–3082

Fu X, Wang B, Li T, McCreary JP (2003) Coupling between northward propagating, intraseasonal oscillations and sea-surface temperature in the Indian Ocean. J Atmos Sci 60:1733–1783

Gadgil S (2003) The Indian Monsoon and its variability. Annu Rev Earth Planet Sci 31:429–467

Gopalakrishna VV, Durand F, Nisha K, Lengaigne M, Costa J, Rao RR, Ravichandran M, Amrithash S, John L, Girish K, Ravichandran C, Suneel V (2009) Observed intra-seasonal to interannual variability of the upper ocean thermal structure in the South-Eastern Arabian Sea during 2002–2008. Deep Sea Res 57:739–754

Gopalan AKS, GopalaKrishna VV, Ali MM, Sharma R (2000) Detection of Bay of Bengal eddies from TOPEX and insitu observations. J Mar Res 58:721–734

Goswami BN (2005) South Asian Monsoon. In: Lau WKM, Waliser DE (eds) Intraseasonal variability in the atmosphere-ocean climate system. Praxis Springer, Berlin, pp 19–55

Goswami BN, Ajaya Mohan RS (2001) Intraseasonal oscillations and interannual variability of the Indian summer monsoon. J Clim 14:1180–1198

Griffies SM, Hallberg RW (2000) Biharmonic friction with a Smagorisky viscosity for use in large scale eddy-permitting ocean models. Mon Wea Rev 128:2935–2946

Hendon HH, Glick J (1997) Intraseasonal Air-Sea interaction in the Tropical Indian and Pacific Oceans. J Clim 10:647–662

Ingram KT, Roncoli MC, Kirshen PH (2002) Opportunities and constraints for farmers of west Africa to use seasonal precipitation forecasts with Burkina Faso as a case study. Agr Syst 74:331–349

Jayakumar A, Vialard J, Lengaigne M, Gnanaseelan C, McCreary JP, Praveen Kumar B (2011) Processes controlling the surface temperature signature of the Madden-Julian Oscillation in the thermocline ridge of the Indian Ocean. Clim Dyn (in press)

Joseph PV, Sabin TP (2008) An ocean–atmosphere interaction mechanism for the active break cycle of the Asian summer monsoon. Clim Dyn 30:553–566

Joseph PV, Sijikumar S (2004) Intraseasonal variability of the low-level jet stream of the Asian summer monsoon. J.Clim. 17:1449–1458

Kalnay et al (1996) The NCEP/NCAR 40-year reanalysis project. Bull Am Meteor Soc 77:437–470

Kanamitsu M, Ebisuzaki W, Woollen J, Yang S-K, Hnilo JJ, Fiorino M, Potter GL (2002) NCEP-DEO AMIP-II Reanalysis (R-2), Bul Atmos Met Soc 1631-1643

Krishnamurti TN, Oosterhof DK, Mehta AV (1988) Air-Sea interaction on the time scale of 30 to 50 days. J Atmos Sci 45:1304–1322

Large WG, Yeager SG (2004) Diurnal to decadal global forcing for ocean and sea-ice models: the data sets and flux climatologies NCAR/TN-460+STR, 111 pp

Large WG, McWilliams JC, Doney SC (1994) Oceanic vertical mixing: a review and a model with a no local boundary layer parametrization. Rev Geophys 32:363–403

Lawrence DM, Webster PJ (2002) The boreal summer intraseasonal oscillation: relationship between eastward and northward movement of convection. J Atmos Sci 59:1593–1606

Levitus S (1998) Climatological atlas of the world ocean, Tech Rep, NOAA, Rockville, Md

Locarnini RA, Mishonov AV, Antonov JI, Boyer TP, Garcia HE, Baranova OK, Zweng MM, Johnson DR (2010) World Ocean Atlas 2009, vol 1: Temperature. S. Levitus (ed) NOAA Atlas NESDIS 68. U.S. Government Printing Office, Washington, D.C.

Prasad TG (2004) A comparison of mixed-layer dynamics between the Arabian Sea and Bay of Bengal: one-dimensional model results. J Geophys Res 109:C03035. doi:10.1029/2003JC002000

Praveen Kumar B, Vialard J, Lengaigne M, Murty VSN, McPhaden MJ (2010) TropFlux: air-sea fluxes for the global tropical oceans—description and evaluation against observations. Clim Dyn (submitted)

Roxy M, Tanimoto Y (2007) Role of SST over the Indian ocean in influencing intraseasonal variability of the Indian summer monsoon. J Met Soc Jpn 85:349–358

Sengupta D, Ravichandran M (2001) Oscillations of Bay of Bengal sea surface temperature during the 1998 summer monsoon. Geophys Res Lett 28:2033–2036

Sengupta D, Goswami BN, Senan R (2001) Coherent intraseasonal oscillations of ocean and atmosphere during the Asian summer monsoon. Geophys Res Lett 28:4127–4130, doi:10.1029/2001GL013587

Seo H, Murtugudde R, Jochum M (2008) Coupled modeling of the oceanatmosphere interactions in the Western Arabian Sea. Ocean Model 25:120–131

Shinoda T, Hendon HH (1998) Mixed layer modeling of intraseasonal variability in the tropical western Pacific and Indian Oceans. J Clim 11:2668–2685

Shenoi SSC, Shankar D, Shetye SR (2002) Differences in heat budgets of the near-surface Arabian Sea and Bay of Bengal: implications for the summer monsoon. J Geophys Res 107:3052. doi:10.1029/2000JC000679

Smith SR, Legler DM, Verzone KV (2001) Quantifying uncertainties in NCEP re-analyses using high-quality research vessel observations. J Clim 14:4062–4072

Thompson B, Gnanaseelan C, Salvekar PS (2006) Variability in the Indian Ocean circulation and salinity and its impact on SST anomalies during dipole events. J Mar Res 64:853–880

Vecchi GA, Harrison DE (2002) Monsoon breaks and subseasonal sea surface temperature variability in the Bay of Bengal. J Clim 15:1485–1493

Vecchi GA, Xie S-P, Fischer A (2004) Air-sea coupling over Western Arabian sea cold filaments. J Clim 17:1213–1224

Vinayachandran PN, Yamagata T (1998) Monsoon response of the sea around Sri Lanka: generation of thermal domes and anticyclonic vortices. J Phys Oceanogr 28:1946–1950

Waliser DE, Murtugudde R, Lucas LE (2004) Indo-Pacific Ocean response to atmospheric intraseasonal variability: 2. Boreal summer and the intraseasonal oscillation. J Geophys Res 109:C03030. doi:10.1029/2003JC002002

Wang B, Webster P, Kikuchi K, Yasunari T, Qi Y (2006) Boreal summer quasi-monthly oscillation in the global tropics. Clim Dyn 27:661–675

Webster PJ, Magana VO, Palmer TN, Shukla J, Tomas RA, Yanai M, Yasunari T (1998) Monsoons: processes, predictability, and the prospects for prediction. J Geophys Res 103:14451–14510

Wentz FJ, Gentemann C, Smith D, Chelton D (2000) Satellite measurements of sea-surface temperature through clouds. Science 288:847–850

Yu L, Weller RA (2007) Objectively analyzed air-sea heat fluxes (OAFlux) for the global oceans. Bull Am Meteor Soc 88:527–539

Zhang Y, Rossow WB, Lacis AA, Oinas V, Mishchenko MI (2004) Calculation of radiative fluxes from the surface to top of atmosphere based on ISCCP and other global data sets: Refinments of the radiative trasfer model and the input data. J Geophys Res 109, doi:10.1029/2003JD004457